ADVANCED MATERIALS TECHNOLOGIES
www.advmattechnol.de

Inkjet-Printed Self-Hosted TADF Polymer Light-Emitting Diodes

Cameron M. Cole, Susanna V. Kunz, Paul E. Shaw, Chandana Sampath Kumara Ranasinghe, Thomas Baumann, James P. Blinco, Prashant Sonar, Christopher Barner-Kowollik, and Soniya D. Yambem**

Thermally activated delayed fluorescent (TADF) materials are extensively investigated as organic light-emitting diodes (OLEDs) with TADF emitting layers demonstrating high efficiency without the use of heavy metal complexes. Therefore, solution-processable and printable TADF emitters are highly desirable, moving away from expensive vacuum deposition techniques. In addition, using emissive materials not requiring an external host simplifies the fabrication process significantly. Herein, OLEDs using a solution-processable TADF polymer that do not need an external host are introduced. The non-conjugated TADF polymer features a TADF emitter (4-(9H-carbazol-9-yl)-2-(3′-hydroxy-[1,1′-biphenyl]-3-yl)-isoindoline-1,3-dione) as a side chain, as well as a hole-transporting side chain and an electron-transporting side chain on an inactive polymer backbone. All organic layers of the OLEDs are fabricated using solution processing methods. The OLEDs with inkjet-printed emissive layers have comparable maximum current and external quantum efficiency as their spin-coated counterparts, exceeding luminance of 2000 cd m^{-2}. The herein-explored strategy is a viable route toward self-hosted printable TADF OLEDs.

1. Introduction

Organic light-emitting diodes (OLEDs) are now widely used in commercial display applications such as smart-phone and television screens. The emergence of OLEDs in commercial products is underpinned by the successful progression of many generations of OLEDs. While successful device designs are possible through combinations of device engineering and material development, the different generations have been marked by the emergence of new types of emissive materials. In terms of emissive materials, OLEDs have progressed through fluorescent and phosphorescent emitters, the first and second generations, respectively. Currently, OLEDs are in their third generation of emissive materials, namely thermally activated delayed fluorescent (TADF) emitters.[1]

TADF technology has shown key promise over the past decade due to its potential to harvest 100% of the electrogenerated excited states (excitons) for emission without the use of heavy-metal complexes.[2] However, the predominant method for fabricating efficient TADF OLEDs is through the expensive process of vacuum deposition, requiring very low pressures and high temperatures. Additionally, a large quantity of material is wasted using this technique and the deposition area is limited by the size of the vacuum chamber. An alternative to vacuum deposition and a potentially low-cost technique is solution processing.

C. M. Cole, S. V. Kunz, J. P. Blinco, P. Sonar, C. Barner-Kowollik, S. D. Yambem
Centre for Materials Science
School of Chemistry and Physics
Queensland University of Technology (QUT)
2 George Street, Brisbane, QLD 4000, Australia
E-mail: christopher.barnerkowollik@qut.edu.au; soniya.yambem@qut.edu.au

The ORCID identification number(s) for the author(s) of this article can be found under https://doi.org/10.1002/admt.202200648.

DOI: 10.1002/admt.202200648

P. E. Shaw, C. S. K. Ranasinghe
Centre for Organic Photonics & Electronics
The School of Chemistry and Molecular Biosciences
The University of Queensland
Brisbane, QLD 4072, Australia

T. Baumann
Cynora GmbH
Werner-von-Siemens-Straße 2–6, 76646 Bruchsal, Germany

C. Barner-Kowollik
Institute of Nanotechnology
Karlsruhe Institute of Technology (KIT)
Hermann-von-Helmholtz-Platz 1
76344 Eggenstein-Leopoldshafen, Germany

Solution processing is a low-temperature process that enables large-area fabrication.[3] Solution-processed TADF OLEDs have reached high external quantum efficiencies (EQEs), >30%.[4] Large-area solution processing is achievable through printing techniques such as inkjet printing. Inkjet printing is a fast and accurate process that enables intricately designed, mask-free, and contactless deposition of functional materials. There is very little to no wastage of materials, rendering inkjet printing one of the more cost-effective deposition methods.[5]

For successful inkjet printing of an emitting material layer (EML), optimization of the ink is critical. Key properties that need to be considered during ink design are surface tension, viscosity, boiling point of the solvent(s), and concentration. Furthermore, for multi-layered solution processing, solubility and solvent orthogonality to the underlying layers are equally important.[6] Due to the specific criteria required for printing, there is a very limited range of suitable solvents for selection. One of the main hurdles for inkjet printing is the low viscosity of inks. The viscosity of inks can be increased by increasing the concentration of the emitting material in the case of polymer emitting materials. This increases the range of solvents that can be selected. However, an increase in the concentration of a small-molecule emitting material (usually ≤1 kg mol^{-1}) has little effect on the ink viscosity.[7] Furthermore, small-molecule light-emitting materials suffer from recrystallization and low solubility compared to their polymeric counterparts.[8]

It is beneficial to incorporate a host material into the emissive layer to facilitate efficient exciton generation (electron-hole pairing) and radiative decay in both phosphorescent and TADF OLEDs.[9] Much like small-molecule light-emitting materials, small-molecule host materials suffer from crystallization and poor solubility, and they are, therefore, not ideal for inkjet printing of the EML.[9] Further, the blending of host materials and emissive materials may lead to other hindrances such as phase separation.[10] To circumvent these issues, a number of self-hosted (single material in EML and no external host material) TADF solution-processed OLEDs made from monomers,[11] dendrimers,[12] and polymers[13] have been reported. Whilst inkjet printing of TADF materials in OLEDs has been achieved,[14] inkjet printing of self-hosted TADF polymers has not yet been accomplished.

In the current study, we report solution-processed OLEDs with a self-hosted TADF polymer emitting layer, which is also printable. In these types of polymers, the emitting, electron-transporting, and hole-transporting moieties are present as pendants/side chains of a non-conjugated backbone. This enables the fabrication of OLEDs without any external hosts, simplifying the fabrication process. Here, we initially compare the performance of our polymer in spin-coated OLEDs with and without an external host material. The OLEDs with only our self-hosted polymer resulted in higher luminance and efficiencies. Finally, we inkjet printed the TADF polymer and fabricated a self-hosted OLED with the same structure as the best-performing spin-coated OLED. The inkjet-printed TADF OLEDs had a luminance of >2000 cd m^{-2}, and to the best of our knowledge, is the first self-hosted inkjet-printed TADF polymer OLED. Our work is a significant step toward simplified inkjet printing of TADF OLEDs and paves the way for large-scale fabrication of TADF OLEDs.

2. Results and Discussion

We recently reported the synthesis and characteristics of different non-conjugated self-hosted TADF polymers.[15] Herein, we have chosen the polymer D3P-DEH (**Figure 1**a) because the transporting side chains of D3P-DEH are derivatives of 1,3-bis(N-carbazolyl)benzene (mCP), which is a well-studied commercially available transport material. In addition, D3P-DEH is one of the polymers, which is synthetically less challenging but at the same time gives almost identical performance to other polymers when tested in single charge carrier devices. D3P-DEH is constituted of 12.7 mol% E1, 43.65 mol% M4, and 43.65 mol% M6, where E1 is the TADF emitting monomer (4-(9H-carbazol-9-yl)-2-(3′-hydroxy-[1,1′-biphenyl]-3-yl)-isoindoline-1,3-dione), M4 carries an mCP pendant group as a hole-transporting species, and the structurally similar M6 employs the electron-transporting α-carboline instead of carbazole in the mCP core (Figure 1a).

In the first part of the study, we compare the performance of D3P-DEH in OLEDs with and without a host. For OLEDs with a host, we selected the (am)bipolar small-molecule 2,6-bis(3-(carbazol-9-yl)phenyl)pyridine (26DCzPPy) (Figure 1b) as the host material. 26DCzPPy has balanced electron and hole mobilities. An advantage of using 26DCzPPy is its solubility in the same solvents as D3P-DEH. In addition, our previous work has demonstrated the compatibility of 26DCzPPy with polymers with the same TADF emitting species as D3P-DEH.[14a,16]

The TADF emitting monomer, E1, as well as other polymers using E1, have been well studied. In polymers containing E1, the highest occupied molecular orbital (HOMO) is ≈–6.1 eV and the lowest unoccupied molecular orbital (LUMO) is ≈–3.2 eV.[17] The electron-transporting monomer (red species in Figure 1a) has a HOMO of ≈–5.6 eV, a LUMO of ≈–2.4 eV, and the lowest-lying excited triplet energy (T_1) of 2.88 eV. The hole-transporting monomer (blue species in Figure 1a) has a HOMO of –5.9 eV, a LUMO of –2.4 eV, and a T_1 of 2.91 eV.[15] Therefore, the HOMO of the hole-transporting monomer M4 and the LUMO of the electron-transporting monomer M6 are similar to the HOMO ($\Delta \approx 0.15$ eV) and the LUMO ($\Delta \approx 0.2$ eV) of 26DCzPPy, respectively. A benefit that these hole and electron-transporting monomers have over 26DCzPPy is that they have a higher T_1 (26DCzPPy T_1 = 2.71 eV), which reduces the transfer of charges away from the emitting species E1.[15]

The absorption and photoluminescence (PL) of thin films of D3P-DEH and D3P-DEH blended with 26DCzPPy (D3P-DEH:26DCzPPy) are shown in Figure 1c. The PL of D3P-DEH has a peak close to 500 nm, while the PL of D3P-DEH:26DCzPPy has a peak at ≈495 nm. The contribution of 26DCzPPy to the PL of the D3P-DEH:26DCzPPy film can be seen as a peak close to 400 nm, which is absent in the PL of the D3P-DEH film. This small contribution of 26DCzPPy, along with the likelihood of reduced concentration quenching of D3P-DEH by the addition of 26DCzPPy, results in a small blue shift of the PL spectrum of D3P-DEH:26DCzPPy (495 nm) compared to the PL of D3P-DEH (500 nm). Concentration quenching is highly feasible for D3P-DEH, as this is common for the emitting moiety E1 in D3P-DEH.[14a] Furthermore, it has previously been shown[14a] that with the addition of 26DCzPPy, there are minimal changes to the TADF properties

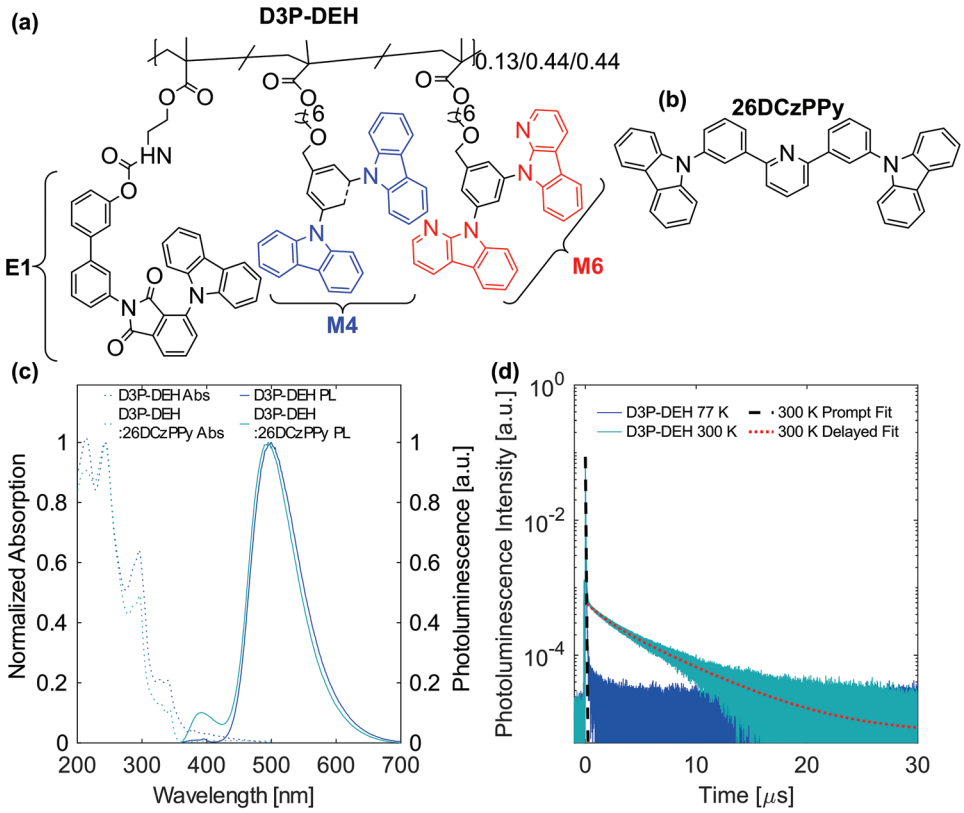

Figure 1. Chemical structures of a) D3P-DEH (hole-transporting species are marked in blue and electron-transporting species are marked in red) and b) 26DCzPPy. c) Absorption and photoluminescence (PL) spectrum of D3P-DEH and D3P-DEH(30 wt%):26DCzPPy, where the films are excited at 290 nm. d) Time-resolved PL of D3P-DEH at 300[15] and 77 K with a tri-exponential fit to the 300 K D3P-DEH data. The time-resolved PL at 300 K in (d) is reproduced with permission.[15] Copyright 2022, Royal Society of Chemistry.

of the emitter. It has also been shown that with the addition of side chains to the polymer (either crosslinking or transporting side chains), there are minimal effects on the TADF properties with this emitter.[17,18]

Time-resolved photoluminescence (TRPL) decay at ambient temperature (300 K)[15] and low temperature (77 K) of D3P-DEH is shown in Figure 1d. A tri-exponential fit to the data measured at 300 K was applied to extract the prompt and delayed lifetimes of D3P-DEH. The prompt component of D3P-DEH, representing the radiative decay from the lowest-lying excited singlet energy level (S_1) to the ground state (S_0) ($S_1 \rightarrow S_0$), has a lifetime (τ_{PF}) of 24.1 ± 0.1 ns (double logarithmic plot TRPL at 300 K is shown in Figure S1, Supporting Information). This prompt lifetime is similar to that of E1 (20.9 ± 0.1 ns) and one of our previously reported E1-based polymers (23.8 ± 0.1 ns).[14a] The average delayed lifetime (τ_{DF}) was calculated from biexponential fits to the decays based on the TADF mechanism, $S_1 \rightarrow T_1 \rightarrow S_1 \rightarrow S_0$. The τ_{DF} for D3P-DEH is relatively short at 4.8 ± 0.1 µs, which can be attributed to the small 0.025 eV energy gap between S_1 and T_1 (ΔE_{ST}) for D3P-DEH (**Table 1**). The small ΔE_{ST} facilitates fast intersystem crossing (ISC) ($S_1 \rightarrow T_1$) and reverse intersystem crossing (RISC)($T_1 \rightarrow S_1$). Rates and rate calculations of ISC (κ_{ISC}) and RISC (κ_{RISC}) for D3P-DEH can be found in Section S1, Supporting Information. The significant reduction in the delayed component of the PL with a decrease in temperature from 300 to 77 K (Figure 1d), indicates that the $T_1 \rightarrow S_1$ process is thermally activated.

The photoluminescence quantum yield (PLQY), Φ_{PL}, of D3P-DEH (Table 1) can be split into its two contributing components using the TRPL fits. The prompt PLQY (Φ_{PF}), and the delayed PLQY (Φ_{DF}) (Table S1, Supporting Information) have nearly an even split, 20.6 ± 1.3% and 23.3 ± 1.5%, respectively. This suggests that only a small portion of the S_1 excitons successfully completed the steps $S_1 \rightarrow T_1 \rightarrow S_1 \rightarrow S_0$, evident in the RISC quantum yield of 29.5 ± 1.9%, compared to the ISC yield of 79.4 ± 8.1%.

Atomic force microscopy (AFM) images of D3P-DEH and D3P-DEH:26DCzPPy spin-coated films are shown in **Figures 2**a,b, respectively. Both D3P-DEH and D3P-DEH:26DCzPPy films have a low root mean square surface roughness (R_q) of 0.407 and 0.904 nm, respectively (average roughness [R_a] of 0.293 nm for D3P-DEH and 0.515 nm for D3P-DEH:26DCzPPy). Whilst the roughness of the D3P-DEH:26DCzPPy film is higher than that of the D3P-DEH film, both of these values are within the

Table 1. Photophysical data, including energy levels, lifetimes, and PLQY, for TADF polymer D3P-DEH in solid state.

	S_1 [eV]	T_1 [eV]	ΔE_{ST} [eV]	τ_{PF} [ns]	τ_{DF} [µs]	Φ_{PL} [%]
D3P-DEH	2.805[15]	2.780[15]	0.025[15]	24.1 ± 0.1	4.8 ± 0.1	44.0 ± 2.8[15]

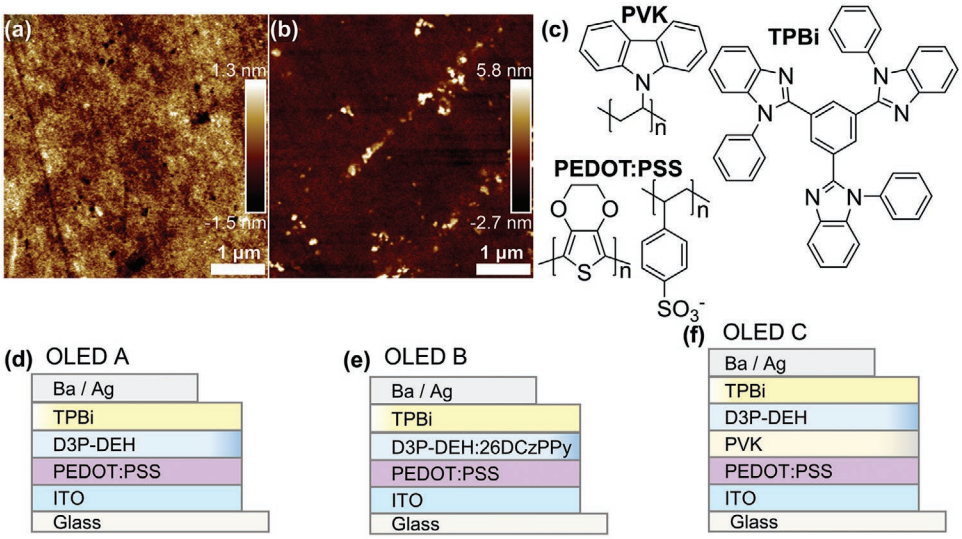

Figure 2. Atomic force images of films of a) D3P-DEH and b) D3P-DEH(30 wt%):26DCzPPy on glass. c) Chemical structures of PVK, TPBi, and PEDOT:PSS. d–f) OLED device structure using D3P-DEH where all organic layers are spin coated. OLED A is self-hosted (no external host) and HTL-free, OLED B has an external host and is HTL-free and OLED C is self-hosted and has an HTL.

expected range for spin-coated thin films. The R_q values for the D3P-DEH:26DCzPPy film is also similar to previous work carried out using a similar polymer blended with 26DCzPPy, which had an R_q value of 0.92 nm over a much larger area (6400 µm^2).[14a]

To investigate the electroluminescent performance of D3P-DEH, a simple OLED device structure was fabricated with either D3P-DEH (OLED A) or D3P-DEH with the host 26DCZPPy (OLED B) as the EML (Figure 2d,e). The other layers in these OLEDs consisted of indium-tin-oxide (ITO), poly(3,4-ethylenedioxythiophene) doped with poly (styrene sulfonate) (PEDOT:PSS), 1,3,5-tris(1-phenyl-1H-benzimidazol-2-yl) benzene (TPBi), barium (Ba), and silver (Ag), as the anode, hole injection layer, electron-transporting layer, electron injection layer, and cathode, respectively. An energy level diagram of all the materials used in the OLED is shown in Figure S2, Supporting Information. All the organic layers were deposited by spin coating for both OLEDs.

The electroluminescence (EL) spectrum (**Figure 3**a) and the Commission Internationale de L'Eclairage (CIE) coordinates (Figure 3b) of OLEDs A and B have minimal difference. The EL peak of OLED B is red-shifted by 6 nm compared to OLED A (509 to 515 nm). However, given the broad peak of EL spectrum for both OLEDs, these peak emission wavelengths should be treated as indicative values as they could be anywhere within ≈10 nm of these values. The full width at half maximum (FWHM) values for the EL spectra are within 5 nm of each other and within the range of what is expected for TADF emitters.[19] FWHM of OLED A and B are 83 and 88 nm, respectively. These small variations in EL could be due to slight changes to the recombination zone from either, variations in film thicknesses, different charge injection barriers, and/or a variation in the mobility within the EML with the addition of 26DCzPPy.

The current–voltage–luminance (*IVL*) relationship and current efficiency (CE) and EQE with respect to luminance are shown in Figure 3c,d. With the addition of a host material, OLED B has a much lower turn-on voltage (V_{on} = ≈5.58 V) than OLED A (V_{on} = ≈7.75 V) (**Table 2**). However, the maximum luminance of OLED B is significantly lower compared to OLED A. OLED A has a maximum luminance of ≈5945 cd m^{-2}, whereas, OLED B's maximum luminance is ≈3600 cd m^{-2}. The EQE and CE of OLED A are more than double that of OLED B. OLED A's maximum EQE and CE are ≈1.57% and ≈5.03%, respectively, whereas, OLED B's EQE and CE are ≈0.62% and ≈1.95%, respectively. One possible explanation for the reduction in luminance, EQE, and CE could be the reduction in emitting moieties within the EML, where OLED A has 10 wt% and OLED B, which has the additional host 26DCzPPy, has only 3 wt% emitting moieties. In experiments with our previously reported polymers that have the same emitting moiety as D3P-DEH, we found that the polymer with a higher mol% of emitting species has higher luminance (Figure S3, Supporting Information).[14a] EQE and CE values of OLEDs A–C at specific luminance are provided in Table S2, Supporting Information.

To reduce the turn-on voltage of the neat D3P-DEH devices (OLED A), a poly(9-vinylcarbazole) (PVK) layer was inserted between PEDOT:PSS and D3P-DEH (OLED C, Figure 2f). The PVK layer acts as a bridge between PEDOT:PSS and D3P-DEH, facilitating better hole injection (Figure S2, Supporting Information).[14b,16] In addition, PVK improves charge and exciton confinement because of its shallow LUMO and high T_1. With the addition of PVK, the V_{on} is reduced from 7.75 ± 0.25 V (OLED A) to 5.73 ± 0.19 V (OLED C) (Table 2). The EL spectrum for OLED C (Figure 3a) is nearly identical to OLED A with an EL peak at 517 nm and an FWHM of 87 nm. Furthermore, there is no loss in luminance. EQE and CE were either the same or improved, with the largest improvement in EQE occurring at 100 cd m^{-2}, increasing from 0.89 ± 0.16% for OLED A to 1.28 ± 0.39% for OLED C. All the OLEDs have high-efficiency roll-off (see Figure 3d), as is typical of many TADF OLEDs.[20] The results for OLED D, a version of OLED B with a PVK layer is provided in the Supporting Information.

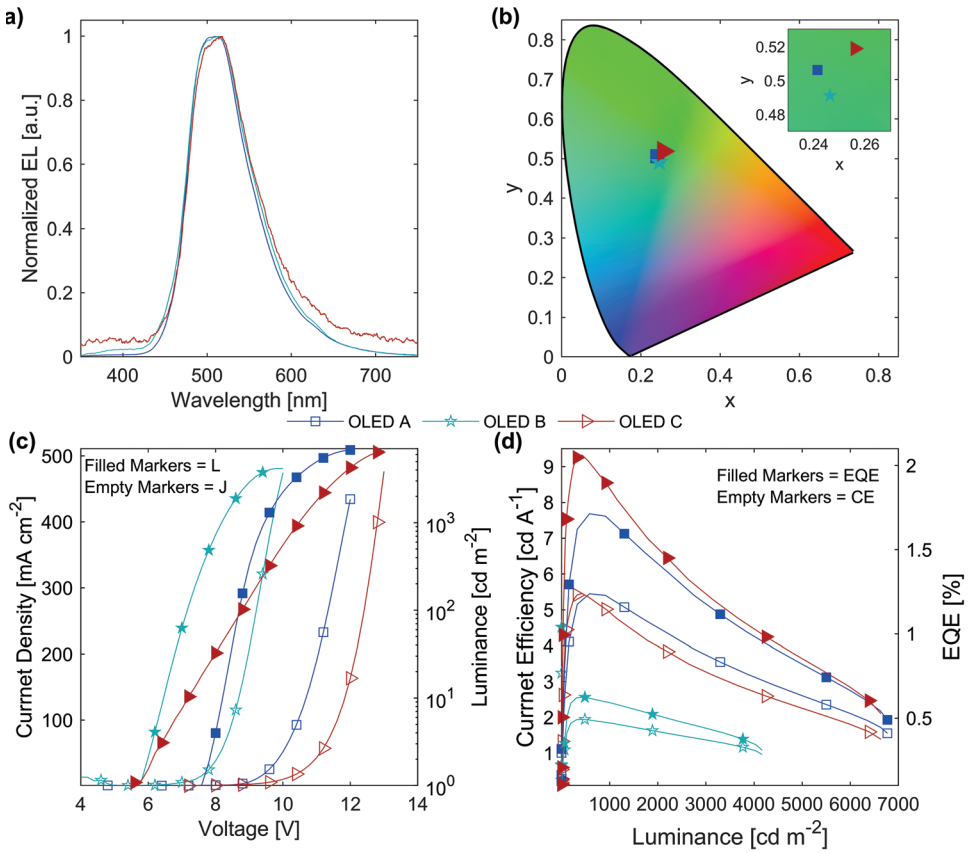

Figure 3. Characteristics of spin-coated OLEDs A, B, and C, where a) is the EL spectrum, b) is the CIE coordinates, c) is the current density and luminance with respect to voltage (filled markers are luminance [*L*] and empty markers are current density [*J*]), and d) is the current efficiency and the EQE with respect to luminance, (filled markers are EQE and empty markers are current efficiency [CE]).

The results from the spin-coated OLEDs study indicate that the performance of neat D3P-DEH OLEDs is comparable to or better than host-containing OLEDs in all parameters. Thus, we subsequently proceeded to fabricate an OLED with an inkjet-printed D3P-DEH EML (OLED E). To produce a D3P-DEH ink, anisole was selected as the main organic solvent, and propylene carbonate (PC) as the co-solvent. For our application, it was imperative to select solvents that could potentially be upscaled, ergo, solvents that are non-halogenated and lower in toxicity. The properties of the ink are also dependent on the viscosity, surface tension, and boiling point of the solvents. Anisole has a high boiling point of 155 °C, a viscosity of 1.01 ± 0.01 mPa s (at 25 °C and a shear rate of 10 s^{-1}),[14a] and surface tension of 35.1 mN m^{-1}(at 20 °C).[21] PC was selected as the co-solvent because of its substantially higher boiling point than anisole (240 °C), which is a desirable property of a co-solvent. The higher boiling point of the co-solvent improves the morphology of printed films, such as reducing the coffee-ring effect.[22] Furthermore, as inkjet printing is considered a slow drying process, the drying time is determined by the boiling point, where the use of a higher boiling point co-solvent reduces the drying rate, which can result in a more uniform film.[22b,23] PC also has a higher viscosity (2.44 ± 0.01 mPa s at 25 °C and a constant shear rate of 10 s^{-1}) and surface tension (41.1 mN m^{-1} at 20 °C).[24]

To generate the inks for inkjet printing, D3P-DEH was dissolved in a blended solvent comprising 95 vol% anisole and 5 vol% PC. The blended solvent of anisole (95 vol%): PC has an average viscosity of 1.03 ± 0.01 mPa s (25 °C) at the constant shear rate of 10 s^{-1}. This average viscosity did not change with an increase in the shear rate of up to 1000 s^{-1} (**Figure 4**a). With the small amount of D3P-DEH introduced to make the

Table 2. Electroluminescent properties, including turn-on voltage, maximum luminance, maximum EQE, maximum CE, EL peak, FWHM, and CIE coordinates, of OLEDs A, B, and C.

OLEDs	V_{on} [V][a)]	L_{max} [cd m^{-2}][b)]	EQE_{max} [%][c)]	CE_{max} [cd A^{-1}][d)]	EL Peak [nm]	FWHM [nm]	CIE [*x*, *y*]
A	7.75 ± 0.25	5945 ± 1333	1.57 ± 0.27	5.03 ± 0.87	509	83	0.24, 0.51
B	5.58 ± 0.19	3611 ± 296	0.62 ± 0.07	1.95 ± 0.21	515	88	0.25, 0.49
C	5.73 ± 0.19	5906 ± 839	1.71 ± 0.31	4.88 ± 0.88	517	87	0.26, 0.52

[a)]Voltage at the luminance of 1 cd m^{-2}; [b)]Maximum luminance; [c)]Maximum EQE; [d)]Maximum CE.

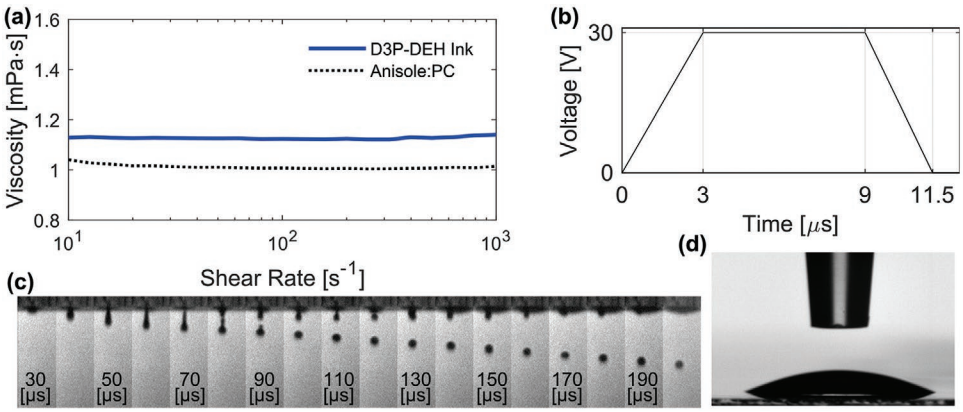

Figure 4. a) Viscosity versus the shear rate of anisole (95vol%):PC (black dots) and D3P-DEH ink (blue line). b) Trapezoidal waveform used for printing D3P-DEH. c) Stroboscopic images (10 µs intervals) of D3P-DEH ink printed with the trapezoidal waveform in (b), and d) D3P-DEH ink droplet used for contact angle measurements.

D3P-DEH ink, the viscosity increased to 1.13 ± 0.00 mPa s (25 °C) for the same constant shear rate. Similar to the blended solvent, the viscosity of D3P-DEH ink did not vary over a range of different shear rates. The D3P-DEH inks have an average contact angle of 14.2 ± 0.8°, which indicates that the ink has good wettability on the underlying layer, which is important to enable ideal film properties (Figure 4d). Furthermore, the surface tension of the ink was similar to that of PC, having a surface tension of 42.8 ± 1.2 1 mN m^{-1} at ≈25 °C.

For inkjet printing of the D3P-DEH ink, a simple trapezoidal waveform was developed (Figure 4b) with a 3 µs rise time, 6 µs dwell time, and a 2.5 µs fall time. The voltage range was set to 30 V, which with a 50 µm print head, produced a droplet with a diameter of ≈40 µm, and volume of ≈30 pL, at a drop speed of ≈1 m s^{-1}. The droplet stroboscopic images are shown in Figure 4c ranging from 30 to 200 µs (each image was taken at 10 µs intervals). At 70 µs, the droplet has a large tail, which is typical of inks that contain polymers. Next, at 80 µs, the tail breaks from the print head, and a small satellite droplet is formed (also seen in the 90 µs frame). However, this satellite re-joins the main droplet by the time it reaches 100 µs. From this point, all droplets continue to drop consistently with minor variations in size and speed.

Subsequently, the D3P-DEH ink was printed onto an ITO/PEDOT:PSS/PVK film. The printhead and print-bed temperatures were set to 25 °C to slow the drying process of the droplets. An array of 90 µm droplet spacing was printed and then annealed at 150 °C. Confocal microscopy and AFM images of a post-annealed printed film are shown in **Figures 5**a,b, respectively. The confocal image shows that the printed film is relatively uniform over an area equivalent to the area of OLEDs fabricated for this study. From the AFM image, the film has an R_q of 9.47 nm and a R_a of 7.25 nm. These films are rougher than the spin-coated D3P-DEH films on glass. The increased roughness of printed films could be due to agglomerations induced by the high annealing temperature of 150 °C.[8] Nonetheless, this film was successfully used in making OLED E, with the remainder of the OLED fabrication following the same steps as the spin-coated OLEDs.

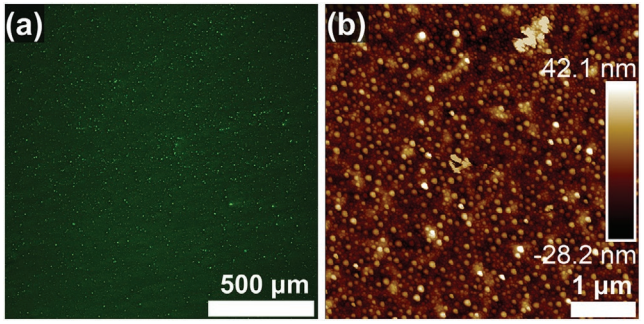

Figure 5. a) Confocal microscopy image of the D3P-DEH inkjet-printed film on ITO/PEDOT:PSS/PVK and b) AFM image of the same film.

The EL spectrum and CIE coordinates of OLED E are shown in **Figures 6**a,b, respectively. There is minimal difference between the EL properties of OLED E and OLED C (spin-coated counterpart), with the EL peak of OLED E at 516 nm, FWHM of 89 nm, and CIE coordinates of 0.27 and 0.50 (**Tables** 2 and **3**). *IVL* characteristics and EQE and CE with respect to the brightness of OLED E are shown in Figures 6c,d, respectively. The V_{on} is ≈3.5 V, which is lower than that of spin-coated OLEDs. This could be attributed to variations in the film thickness or roughness of the EML between printed and spin-coated films. The higher current density of OLED E (Figure 6c) than OLED C (Figure 3c) is also an indicator that the thickness of the OLED has been reduced. The printed OLED reached a maximum luminance of ≈2175 cd m^{-2}. The maximum EQE of ≈1.58% for OLED E is only slightly lower than and within the standard deviation of the maximum EQE of spin-coated OLED C. Overall, the inkjet-printed OLED data indicates that a TADF polymer containing host moieties is an effective strategy toward printed TADF OLEDs.

3. Conclusions

In summary, we have employed a TADF polymer emissive layer in OLEDs with fully solution-processed organic layers. The TADF polymer, D3P-DEH, which features three different side-chain entities consisting of a TADF emitter, an electron conducting side chain, and a hole conducting side chain was first studied using spin coating as the OLED fabrication method.

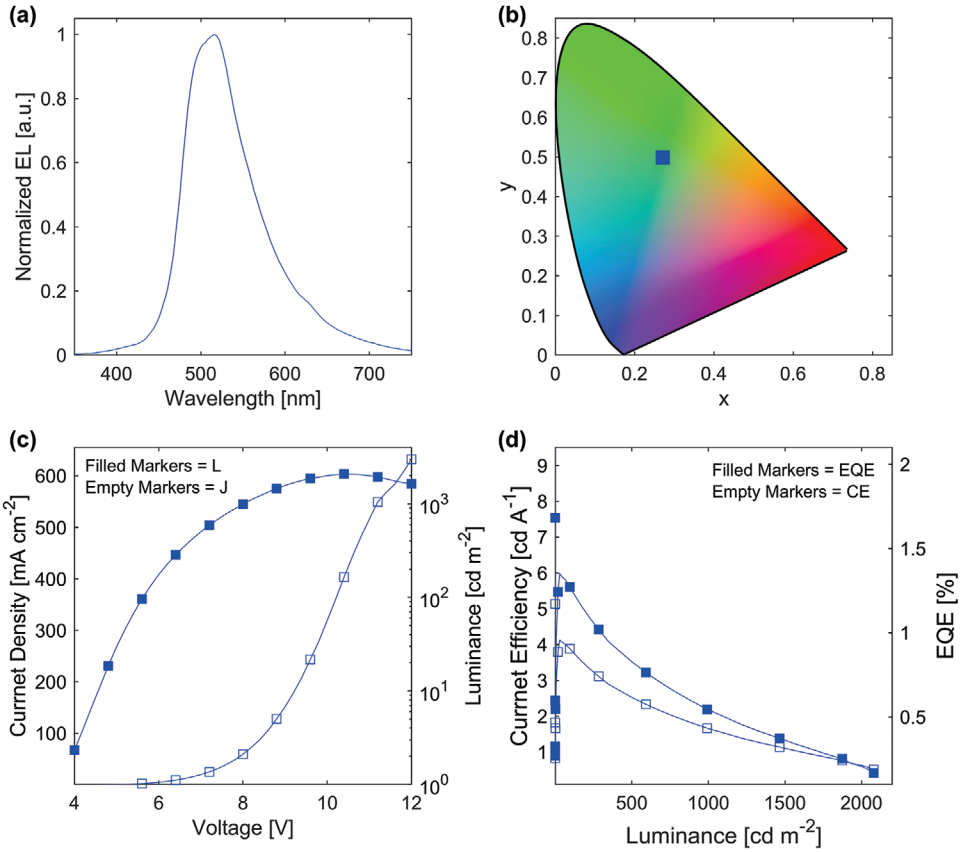

Figure 6. Characteristics of OLED with D3P-DEH inkjet emissive layer, where a) is the EL spectrum, b) is the CIE coordinates, c) is the current density and luminance with respect to voltage (filled markers are luminance [*L*] and empty markers are current density [*J*]), and d) is the current efficiency and the EQE with respect to luminance, (filled markers are EQE and empty markers are current efficiency [CE]).

Spin-coated OLEDs with neat D3P-DEH in the emissive layer showed significantly higher luminance (≈5900 cd m^{-2}) as compared to an OLED with an emissive layer of D3P-DEH mixed with a commercial host, 26DCzPPy (≈3600 cd m^{-2}). Inclusion of an HTL of PVK between PEDOT:PSS and the emissive layer reduced the turn-on voltage of neat D3P-DEH OLEDs by ≈2 V and also increased the maximum EQE. This OLED structure was used for demonstrating an OLED with an inkjet-printed emissive layer. In terms of inkjet printing, a D3P-DEH-only ink displayed good wettability and viscosity, and emissive layers were successfully printed using a simple trapezoidal waveform. An OLED with a printed film showed a negligible loss in maximum EQE as compared to its spin-coated counterpart. To the best of our knowledge, our study introduces the first OLED with a self-hosted inkjet-printed TADF polymer emissive layer. Future studies implementing a more elaborate device structure or a different TADF emitter could further improve efficiencies. Overall, our results indicate that the incorporation of host and emitting species as side chains on a polymer is a promising strategy to improve inkjet printing of TADF materials in OLEDs.

Table 3. Electroluminescent properties of OLEDs A, B, and C.

OLEDs	V_{on} [V][a)]	L_{max} [cd m^{-2}][b)]	EQE_{max} [%][c)]	CE_{max} [cd A^{-1}][d)]	EL Peak [nm]	FWHM [nm]	CIE [*x*, *y*]
E	6.08 ± 0.28	2175 ± 447	1.58 ± 0.34	4.87 ± 1.04	516	89	0.27, 0.50

[a)]voltage at the luminance of 1 cd m^{-2}; [b)]maximum luminance; [c)]maximum EQE; [d)]maximum CE.

4. Experimental Section

OLEDs were fabricated using simple device structures shown in Figure 2. Glass substrates patterned with ITO (Xin Yan Technology Ltd.) were cleaned by wiping with acetone before ultrasonicating in deionized water mixed with lab detergent (Alconox). The substrates were then scrubbed with lab detergent in deionized water before sequential ultrasonication in deionized water, acetone, and isopropanol with each step separated by drying with compressed air. PEDOT:PSS (Heraeus Clevios, AI 4083) was filtered with a 0.45 µm PVDF filter (Kinesis Australia Pty. Ltd., ESF-PVH-13-045) and spin coated (Laurell Technologies Corporation, WS-650MZ-23NPP) at 5000 rpm for 30 s to deposit a 30.9 ± 2.5 nm film. The contacts were exposed by rubbing off with deionized water before annealing on a hotplate at 125 °C for 20 min. The PEDOT:PSS-coated substrates were then transferred into a series of glove boxes with low O_2 (<10 ppm) and H_2O (<0.1 ppm). For the OLEDs with an HTL, PVK (Sigma-Aldrich, 182605) was dissolved in chlorobenzene (CB) (Sigma-Aldrich, 284513) to give a concentration of 10 mg mL^{-1}. The PVK was then spin coated (Specialty coating systems Inc., G3P) at 2000 rpm for 30 s, and contacts were rubbed with CB before annealing at 150 °C for 20 min. The PVK film had a thickness of 18.1 ± 1.0 nm.

The spin-coated EML was prepared by making separate solutions of D3P-DEH and 26DCzPPy (Lumtec, LT-N491) in chloroform ($CHCl_3$) (Sigma-Aldrich, 288306) at a concentration of 5 mg mL^{-1}. For the EML with the host, the two solutions were blended to make a D3P-DEH(30 wt%):26DCzPPy solution and spin coated at 1500 rpm for 30 s to produce a 20.2 ± 2.2 nm film. For the self-hosted OLEDs, the same spin speed parameters were used with this producing an 18.6 ± 0.6 nm film. The contacts were cleaned with CB and annealed for 15 min at 60 °C.

The ink for inkjet printing of EML ink was prepared inside a glove box before the ink and substrates were removed for printing in ambient conditions. A D3P-DEH ink was formulated with a blend of two solvents, 95 vol% anisole (Sigma-Aldrich, 296295) and 5 vol% propylene carbonate (Sigma-Aldrich), to make a 2.5 mg mL^{-1} of ink. Prior to loading the ink into the printer, it was filtered with a 0.22 µm PTFE filter (Kinesis Australia Pty. Ltd., ESF-PT-13-022). Inkjet printing was achieved using a piezoelectric drop-on-demand inkjet printer (MicroFab, Jet-Lab 4XL) with a 50 µm print head device. The printed substrates were annealed for 20 min at 150 °C before being returned to the glove box for the remainder of the fabrication.

Following the deposition of the EML, either through inkjet printing or spin coating, a 1,3,5-tris(1-phenyl-1H-benzimidazol-2-yl)benzene (TPBi) (Lumtec, LT-E302) layer was deposited by spin coating a 4 mg mL^{-1} solution of TPBi in ethanol (Sigma-Aldrich, 459836) at 1000 rpm to produce a 22.4 ± 4.2 nm film. The TPBi film was then removed from the contacts and annealed for 20 min at 50 °C. Finally, Ba (Sigma-Aldrich, 474711) and Ag (Sigma-Aldrich, 474711) were evaporated using a thermal torpedo evaporator at a pressure of $<10^{-6}$ mbar and at a rate of <0.2 Å s^{-1} to produce a ≈5 nm Ba film and a ≈100 nm Ag film. A mask was used for the Ba/Ag evaporation to give a 2 mm^2 OLED.

IVL and EL measurements were done inside the glove box. The *IVL* measurements were recorded using a custom-built set-up using a semiconductor analyzer (Keysight, B1500A) and a calibrated photo-diode (calibrated to a luminance meter (Konica Minolta, CS-200)). The EL measurements were recorded on a UV–vis spectrometer (Ocean Optics, USB 2000+). At least six OLED devices were analyzed for each type of OLED.

Imaging of the inkjet-printed films was done using a confocal microscope (Nikon, A1R Confocal) at 10× magnification using a 405 nm DAPI laser. Film topology and roughness measurements were recorded using AFM (Bruker, Dimension Icon AFM). The AFM data was analyzed using Nano Scope Analysis (Bruker). The film thicknesses were measured using a stylus profilometer (Bruker, Dektak).

The rheology measurements were conducted on a rheometer (Anton Parr, M302 rheometer) using a double gap (DG26) measurement system. Two separate measurements were recorded, one with an increasing shear rate from 10 to 1000 s^{-1}, and another with a consistent shear rate of 10 s^{-1}. The contact angle of the ink onto the ITO/PEDOT:PSS/PVK film, as well as the surface tension of the ink, was recorded using a drop shape analyzer (Biolin, Theta Flex) using 1 µL droplets at room temperature (≈25 °C).

The PL and absorption measurements were recorded using a fluorescence spectrometer (Agilent, Cary Eclipse) with an excitation wavelength of 290 nm and a UV–vis (Agilent, Cary 60), respectively. D3P-DEH and D3P-DEH(30 wt%):26DCzPPy were spin coated onto quartz substrates (Xin Yan Technology Ltd.) for the PL and absorption measurements.

Finally, the low-temperature TRPL was measured using a custom-built spectrometer.[25] The setup included a photomultiplier tube (Hamamatsu, H10721-21) and an ICCD camera (Andor New iStar ICCD), which were connected to an oscilloscope (Teledyne WavePro; 2 Ghz, WavePro 7200A). Samples were kept at 77 K in a cryostat (Oxford Instruments; Optistat DN2 liquid N_2 cryostat) and were cooled with liquid nitrogen. A pulsed laser (Opolette 355 LD; 10 ns, repetition rate 10 Hz, 10 µJ per pulse, Nd:YAG) with an excitation wavelength of 355 nm was used to excite the samples. To reduce the effects of scattered excitation on the emission, the emission was collected at a right angle through a 375 nm long-pass filter.

Supporting Information

Supporting Information is available from the Wiley Online Library or from the author.

Acknowledgements

C.B.-K., J.P.B., P.S., and S.D.Y. acknowledge funding in the context of an Australian Research Council (ARC) Linkage project LP170100387. C.B.-K. is grateful for an ARC Laureate Fellowship enabling his photochemical research program, as well as continued key support from the Queensland University of Technology (QUT). P.S. is thankful for an ARC Future Fellowship. The Central Analytical Research Facility (CARF) at QUT is gratefully acknowledged for access to analytical instrumentation.

Open access publishing facilitated by Queensland University of Technology, as part of the Wiley - Queensland University of Technology agreement via the Council of Australian University Librarians.

Conflict of Interest

The authors declare no conflict of interest.

Data Availability Statement

The data that support the findings of this study are available from the corresponding author upon reasonable request.

Keywords

inkjet printing, organic light-emitting diodes, self-hosted, solution processing, thermally activated delayed fluorescence, thermally activated delayed fluorescent polymers

Received: April 20, 2022
Revised: May 26, 2022
Published online:

[1] J. H. Lee, C. H. Chen, P. H. Lee, H. Y. Lin, M. K. Leung, T. L. Chiu, C. F. Lin, *J. Mater. Chem. C* **2019**, *7*, 5874.
[2] a) A. Endo, K. Sato, K. Yoshimura, T. Kai, A. Kawada, H. Miyazaki, C. Adachi, *Appl. Phys. Lett.* **2011**, *98*, 083302; b) A. Endo, M. Ogasawara, A. Takahashi, D. Yokoyama, Y. Kato, C. Adachi, *Adv. Mater.* **2009**, *21*, 4802; c) Q. Zhang, D. Tsang, H. Kuwabara, Y. Hatae, B. Li, T. Takahashi, S. Y. Lee, T. Yasuda, C. Adachi, *Adv. Mater.* **2015**, *27*, 2096.
[3] L. A. Duan, L. D. Hou, T. W. Lee, J. A. Qiao, D. Q. Zhang, G. F. Dong, L. D. Wang, Y. Qiu, *J. Mater. Chem.* **2010**, *20*, 6392.
[4] K.-W. Tsai, M.-K. Hung, Y.-H. Mao, S.-A. Chen, *Adv. Funct. Mater.* **2019**, *29*, 1901025.
[5] T. Y. Huang, W. Jiang, L. Duan, *J. Mater. Chem. C* **2018**, *6*, 5577.
[6] M. J. J. Coenen, T. M. W. L. Slaats, T. M. Eggenhuisen, P. Groen, *Thin Solid Films* **2015**, *583*, 194.
[7] S. Meyer, M. Hamburger, S. Stolz, M. Engel, A. Hayer, H.-R. Tseng, R. Linge, R. Anémian, in *Advanced Display Technology: Next Generation Self-Emitting Displays*, (Eds: I. B. Kang, C. W. Han, J. K. Jeong), Springer Singapore, Singapore **2021**.
[8] L. Zhou, L. Yang, M. J. Yu, Y. Jiang, C. F. Liu, W. Y. Lai, W. Huang, *ACS Appl. Mater. Interfaces* **2017**, *9*, 40533.

[9] T. Chatterjee, K.-T. Wong, *Adv. Opt. Mater.* **2019**, *7*, 1800565.
[10] S. Wang, H. Zhang, B. Zhang, Z. Xie, W.-Y. Wong, *Mater. Sci. Eng. R Rep.* **2020**, *140*, 100547.
[11] Y. Wada, K. Shizu, S. Kubo, T. Fukushima, T. Miwa, H. Tanaka, C. Adachi, H. Kaji, *Appl. Phys. Express* **2016**, *9*, 032102.
[12] K. Albrecht, K. Matsuoka, K. Fujita, K. Yamamoto, *Angew. Chem., Int. Ed.* **2015**, *54*, 5677.
[13] a) Y. Zhu, Y. Zhang, B. Yao, Y. Wang, Z. Zhang, H. Zhan, B. Zhang, Z. Xie, Y. Wang, Y. Cheng, *Macromolecules* **2016**, *49*, 4373; b) J. Luo, G. Xie, S. Gong, T. Chen, C. Yang, *Chem. Commun.* **2016**, *52*, 2292; c) S. Shao, J. Hu, X. Wang, L. Wang, X. Jing, F. Wang, *J. Am. Chem. Soc.* **2017**, *139*, 17739.
[14] a) C. M. Cole, S. V. Kunz, P. E. Shaw, N. P. Thoebes, T. Baumann, E. Blasco, J. P. Blinco, P. Sonar, C. Barner-Kowollik, S. D. Yambem, *J. Mater. Chem. C* **2020**, *8*, 13001; b) A. C., B. Luszczynska, M. Z. Szymanski, J. Ulanski, K. Albrecht, K. Yamamoto, *Org. Electron.* **2019**, *74*, 218; c) A. Verma, D. M. Zink, C. Fléchon, J. L. Carballo, H. Flügge, J. M. Navarro, T. Baumann, D. Volz, *Appl. Phys. A* **2016**, *122*, 191; d) M. Wallesch, A. Verma, C. Fléchon, H. Flügge, D. M. Zink, S. M. Seifermann, J. M. Navarro, T. Vitova, J. Göttlicher, R. Steininger, L. Weinhardt, M. Zimmer, M. Gerhards, C. Heske, S. Bräse, T. Baumann, D. Volz, *Chem. Eur. J.* **2016**, *22*, 16400.
[15] S. V. Kunz, C. M. Cole, S. C. Gauci, P. E. Shaw, C. S. K. Ranasinghe, T. Baumann, P. Sonar, S. D. Yambem, E. Blasco, C. Barner-Kowollik, J. P. Blinco, *Polym. Chem.* **2022**, https://doi.org/10.1039/d2py00511e.
[16] Y.-S. Tsai, L.-A. Hong, F.-S. Juang, C.-Y. Chen, *J. Lumin.* **2014**, *153*, 312.
[17] S. V. Kunz, C. M. Cole, A. Welle, P. E. Shaw, P. Sonar, N. P. Thoebes, T. Baumann, S. D. Yambem, E. Blasco, J. P. Blinco, C. Barner-Kowollik, *Macromolecules* **2019**, *52*, 9105.
[18] S. V. Kunz, C. M. Cole, T. Baumann, P. Sonar, S. D. Yambem, E. Blasco, C. Barner-Kowollik, J. P. Blinco, *Polym. Chem.* **2021**, *12*, 8.
[19] J. M. Teng, Y. F. Wang, C. F. Chen, *J. Mater. Chem. C* **2020**, *8*, 11340.
[20] M. Hasan, S. Saggar, A. Shukla, F. Bencheikh, J. Sobus, S. K. M. McGregor, C. Adachi, S.-C. Lo, E. B. Namdas, *Nat. Commun.* **2022**, *13*, 254.
[21] a) J. J. Jasper, *J. Phys. Chem. Ref. Data* **1972**, *1*, 841; b) Merk Sigma-Aldrich, Safety data sheet anisole, https://www.sigmaaldrich.com/AU/en/sds/sial/296295 (accessed: January 2022).
[22] a) A. Teichler, R. Eckardt, C. Friebe, J. Perelaer, U. S. Schubert, *Thin Solid Films* **2011**, *519*, 3695; b) A. Teichler, J. Perelaer, U. S. Schubert, *J. Mater. Chem. C* **2013**, *1*, 1910.
[23] A. C., M. Z. Szymański, B. Łuszczyńska, J. Ulański, *Sci. Rep.* **2019**, *9*, 8493.
[24] a) N. L. Jarvis, W. Zisman, *J. Phys. Chem.* **1960**, *64*, 150; b) Merk Sigma-Aldrich, Safety data sheet propylene carbonate, https://www.sigmaaldrich.com/AU/en/sds/sial/310328 (accessed: January 2022).
[25] E. V. Puttock, C. S. K. Ranasinghe, M. Babazadeh, J. Jang, D. M. Huang, Y. Tsuchiya, C. Adachi, P. L. Burn, P. E. Shaw, *Macromolecules* **2020**, *53*, 10375.